Space–Guides: Efficient Thin–Film Optical Interconnects

E. Ertekin and A. Lakhtakia

CATMAS — Computational and Theoretical Materials Sciences Group
Department of Engineering Science and Mechanics
Pennsylvania State University, University Park, PA 16802–6812, USA
Fax: +1 814 863 7967; email: AXL4@psu.edu

Abstract

Waveguiding in a thin–film helicoidal bianistropic medium (TFHBM) layer is investigated. A dielectric TFHBM layer bounded by isotropic dielectric half–spaces is shown to support guided wave propagation with guide wavenumbers dependent on the direction of signal propagation, thus signalling potential use as a space–guide. The modal fields and power transmission distributions associated with the guided modes in the proposed TFHBM interconnects are detailed.

1. Introduction

Implementation of optoelectronic devices requires the development of optical interconnects which, in addition to providing effective signal transmission, must be simple to fabricate on integrated circuitry. In this paper, we present a theoretical study which indicates that dielectric thin–film helicoidal bianisotropic mediums (TFHBMs) are very suitable for realizing optical interconnects. In fact, the adoption of dielectric TFHBM interconnects may result in efficient use of semiconductor real–estate in electronic chips.

2. Theory in Brief

Suppose a linear, dielectric TFHBM layer completely fills the region $|z| \le D/2$, while the halfspaces $z \le -D/2$ and $z \ge D/2$ are filled by an isotropic dielectric medium whose relative permittivity scalar at angular frequency ω is denoted by $\epsilon_r(\omega)$. The constitutive relation $\mathbf{D}(\mathbf{r},\omega) = \epsilon_0 \, \underline{\underline{\epsilon}}(z,\omega) \cdot \mathbf{E}(\mathbf{r},\omega)$ of the TFHBM layer contains the relative permittivity dyadic

$$\underline{\underline{\epsilon}}(z,\omega) = \underline{\underline{S}}_z(z - \tfrac{D}{2}) \cdot \underline{\underline{S}}_y(\chi) \cdot \underline{\underline{\epsilon}}^{\circ}_{ref}(\omega) \cdot \underline{\underline{S}}_y^T(\chi) \cdot \underline{\underline{S}}_z^T(z - \tfrac{D}{2})\,. \tag{1}$$

Here, the *reference* relative permittivity dyadic

$$\underline{\underline{\epsilon}}^{\circ}_{ref}(\omega) = \epsilon_a(\omega)\mathbf{u}_z\mathbf{u}_z + \epsilon_b(\omega)\mathbf{u}_x\mathbf{u}_x + \epsilon_c(\omega)\mathbf{u}_y\mathbf{u}_y\,, \tag{2}$$

where $\mathbf{u}_{x,y,z}$ are the cartesian unit vectors and $\epsilon_{a,b,c}(\omega)$ are frequency–dependent scalars. The rotational non–homogeneity (along the z axis) of a structurally right–handed TFHBM is expressed by the dyadic

$$\underline{\underline{S}}_z(z) \;=\; (\mathbf{u}_x\mathbf{u}_x + \mathbf{u}_y\mathbf{u}_y)\,\cos\left(\frac{\pi z}{\Omega}\right) + (\mathbf{u}_y\mathbf{u}_x - \mathbf{u}_x\mathbf{u}_y)\,\sin\left(\frac{\pi z}{\Omega}\right) + \mathbf{u}_z\mathbf{u}_z \tag{3}$$

with 2Ω as the structural period. The so–called angle of rise χ appears in the tilt dyadic

$$\underline{\underline{S}}_y(\chi) = (\mathbf{u}_x\mathbf{u}_x + \mathbf{u}_z\mathbf{u}_z)\,\cos\chi + (\mathbf{u}_z\mathbf{u}_x - \mathbf{u}_x\mathbf{u}_z)\,\sin\chi + \mathbf{u}_y\mathbf{u}_y\,; \tag{4}$$

typically $\chi \geq 20^\circ$ for the sculptured thin films. Guided wave propagation is ensured if $\epsilon_r < \min\{\epsilon_a,\, \epsilon_b,\, \epsilon_c\}$, with both mediums assumed non–dissipative at the frequency of interest.

Knowing the constitutive relations of the chosen TFHBM layer, we can determine the guide wavenumbers which enable guided wave propagation. A specific guided wave mode can be delineated with the following equations:

$$\left.\begin{array}{rcl} \mathbf{E}(\mathbf{r}) &=& \exp\left[i\kappa\,(x\cos\psi + y\sin\psi)\right]\quad \mathbf{e}(z,\kappa,\psi) \\ \mathbf{H}(\mathbf{r}) &=& \exp\left[i\kappa\,(x\cos\psi + y\sin\psi)\right]\quad \mathbf{h}(z,\kappa,\psi) \end{array}\right\}, \quad -\infty \leq z \leq \infty\,. \tag{5}$$

Here, the angle ψ denotes the propagation direction $\mathbf{u}_\ell = \mathbf{u}_x\cos\psi + \mathbf{u}_y\sin\psi$, while κ is the modal guide wavenumber whose values have to be determined.

The leakage fields accompanying a guided wave mode are represented by

$$\left.\begin{array}{rcl} \mathbf{E}(\mathbf{r}) &=& (b_s\mathbf{s} + b_p\mathbf{p}_-)\exp\left[i\mathbf{k}_- \bullet (\mathbf{r} + \frac{D}{2}\mathbf{u}_z)\right] \\ \mathbf{H}(\mathbf{r}) &=& \frac{1}{\eta}(b_s\mathbf{p}_- - b_p\mathbf{s})\exp\left[i\mathbf{k}_- \bullet (\mathbf{r} + \frac{D}{2}\mathbf{u}_z)\right] \end{array}\right\}, \quad z \leq -\frac{D}{2} \tag{6}$$

in the lower halfspace, and

$$\left.\begin{array}{rcl} \mathbf{E}(\mathbf{r}) &=& (c_s\mathbf{s} + c_p\mathbf{p}_+)\exp\left[i\mathbf{k}_+ \bullet (\mathbf{r} - \frac{D}{2}\mathbf{u}_z)\right] \\ \mathbf{H}(\mathbf{r}) &=& \frac{1}{\eta}(c_s\mathbf{p}_+ - c_p\mathbf{s})\exp\left[i\mathbf{k}_+ \bullet (\mathbf{r} - \frac{D}{2}\mathbf{u}_z)\right] \end{array}\right\}, \quad z \geq \frac{D}{2}\,, \tag{7}$$

in the upper halfspace, with b_s, b_p, c_s, and c_p as the amplitudes of the perpendicular– and the parallel–polarized components. The various vectors introduced in (6) and (7) are given by

$$\mathbf{s} = \mathbf{u}_z \times \mathbf{u}_\ell\,,\ \mathbf{p}_\pm = \mp\left[1 - (\kappa/k)^2\right]^{1/2}\mathbf{u}_\ell + (\kappa/k)\mathbf{u}_z\,,\ \mathbf{k}_\pm = \kappa\mathbf{u}_\ell \pm \left(k^2 - \kappa^2\right)^{1/2}\mathbf{u}_z\,, \tag{8}$$

where $k = k_0\sqrt{\epsilon_r}$, $\eta = \eta_0/\sqrt{\epsilon_r}$, $k_0 = \omega\sqrt{\epsilon_0\mu_0} = 2\pi/\lambda_0$ is the free–space wavenumber, λ_0 is the free–space wavelength, and $\eta_0 = \sqrt{\mu_0/\epsilon_0}$ is the intrinsic impedance of free space. Guided wave propagation is possible only if $\kappa > k$; otherwise, energy launched into the TFHBM layer must leak into the two halfspaces.

On substituting the constitutive relations and the field expressions above into the time–harmonic Maxwell curl equations $\nabla\times\mathbf{E}(\mathbf{r}) = i\omega\mathbf{B}(\mathbf{r})$ and $\nabla\times\mathbf{H}(\mathbf{r}) = -i\omega\epsilon_0\,\underline{\underline{\epsilon}}(z,\omega)\bullet\mathbf{E}(\mathbf{r})$, a 4×4 matrix ordinary differential equation emerges for the TFHBM layer. Its solution requires the prescription of boundary values through (6) and (7). Our interest lies in determining pairs of (κ,ψ) such that not all of the coefficients b_s, b_p, c_s and c_p are null–valued; thereby the dispersion equation is obtained. For guided wave propagation, values of κ denoted by κ_ψ^r, (r = 1, 2, 3,...), that satisfy the dispersion equation have to be numerically determined, the roots being indexed by the integer r in descending order of their magnitudes.

3. Guide Wavenumbers

We implemented the foregoing procedure using the C programming language and the IMSL C numerical library subroutines for complex linear algebra. The wavelength λ_0 was fixed at 600 nm for all calculations. We tested our computer program for the case of an isotropic, homogeneous, dielectric slab waveguide. Analytical solutions to the dispersion equation of this simple waveguide are well–documented – see, *e.g.*, [1]. Setting $\epsilon_r = 1$, we simulated homogeneity and isotropy by choosing $\epsilon_a = \epsilon_b = \epsilon_c$ and taking the limit $1/\Omega \to 0$. The roots κ^r that we obtained corresponded exactly with the analytical results. Furthermore, the calculated mode shapes and power transmission characteristics of the waveguide also matched the expected power transmission and mode shape plots.

Now let us proceed to the proposed TFHBM interconnect. Most calculations were made with $\{\epsilon_a = 3.8, \epsilon_b = 4.6, \epsilon_c = 3.0\}$, in accordance with data from [2]. In general, the guide wavenumbers show a strong dependence on the propagation direction (see [3,4] for more details). This is illustrated in Figure 1, where the guide wavenumbers are indicated for various ψ for a specific TFHBM interconnect. Thus, the proposed TFHBM interconnect functions as *a space–guide through which signals can be simultaneously transported in different directions with different phase velocities*. This feature emerges from the anisotropic and non–homogeneous nature of TFHBMs, and may be exploited for efficient use of semiconductor real–estate in optoelectronic circuitry.

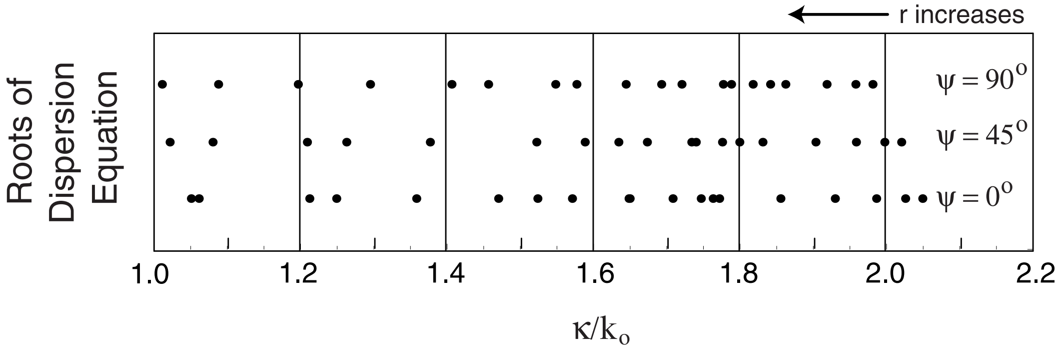

Figure 1: Roots of dispersion equation for directions of propagation denoted by the angle ψ; $\lambda_0 = 600$ nm, $\epsilon_a = 3.0$, $\epsilon_b = 4.6$, $\epsilon_c = 3.8$, $\chi = 30°$, $\Omega = 200$ nm, $D = 8\ \Omega = 1600$ nm.

Independently of all parameters, the guide wavenumbers κ_ψ^r for propagation directions $\mathbf{u}_\ell$ and $-\mathbf{u}_\ell$ are the same. When the TFHBM layer consists of an integral number of periods (*i.e.*, the ratio D/Ω is an even integer), the additional relation $\kappa_\psi^r = \kappa_{\pi-\psi}^r$ holds. This arises because all three principal axes of $\underline{\underline{\epsilon}}(z, \omega)$ rotate through an integral number of turns between the planes $z = -D/2$ and $z = D/2$, thereby imposing a symmetry constraint.

The variability of κ_ψ^r with ψ is most pronounced around the lower values of κ_ψ^r (where solutions of the dispersion equation are more widely spaced). Additionally, the directional–dependence of κ_ψ^r persists for smaller values of D/Ω, including $D/\Omega << 1$. Parenthetically, we also studied the directional–dependence of the guide wavenumbers for a locally uniaxial TFHBM layer with $\{\epsilon_a = \epsilon_c = 3.8, \epsilon_b = 4.6\}$; The guide wavenumbers κ_ψ^r still exhibit a dependence on ψ, but the dependence is weaker than for the biaxial case illustrated in Figure 1.

The number density of guided wave modes is less when D is small. The mode number density appears to be predominantly determined by the overall thickness D, and is largely unaffected by the half–period Ω. Thus, the availability of guided wave modes can be tailored by properly choosing the layer thickness D.

In TFHBM interconnects, κ_ψ^r has an upper bound which varies with ψ. For instance, $\kappa_\psi^r < 2.049\ k_0$ for $\psi = 0°$, whereas $\kappa_\psi^r < 1.981\ k_0$ for $\psi = 90°$, in Figure 1. The upper bound decreases monotonically as ψ increases from 0° to 90°. The upper bound on κ_ψ^r varies with χ, ψ, D, and Ω for given ϵ_a, ϵ_b, and ϵ_c.

4. Space–Guide Modes

The modal fields and power transmission associated with the guided wave modes were also studied. The time–averaged power flow in the propagation direction is given by $P_\ell(z) = \frac{1}{2}\mathbf{u}_\ell \bullet \mathrm{Re}\,[\mathbf{e}(z,\kappa,\psi) \times \mathbf{h}^*(z,\kappa,\psi)]$, where the asterisk denotes the complex conjugate. Detailed numerical study of the modal fields and power distributions revealed that each mode of propagation inside a TFHBM interconnect can be classified into one of two groups: *hybrid electric* (HE) and *hybrid magnetic* (HM). The modes are *hybrid*, because electric and magnetic field components are present in all directions, along the axial ($\mathbf{u}_z$) direction, as well as in the longitudinal and perpendicular directions in the xy plane. This is unlike the modes in an isotropic, dielectric, planar interconnect, wherein the modes are either transverse electric (TE) or transverse magnetic (TM). Another distinction between the HE and HM modes in the TFHBM interconnect and TE and TM modes in the isotropic interconnect is that there appears to be no apparent ordering to the occurence of the HE and HM modes, while the TE and TM modes alternate with $r = 1, 2, 3, \ldots$.

For both the HE and the HM modes, the power transmission distributions $P_\ell(z)$ are quite similar to those of the TE and the TM modes, respectively. In fact, for propagation in any direction, it is possible to order the guided modes HE_n and HM_n, $(n = 1, 2, 3, \ldots)$, based upon the similarity of $P_\ell(z)$, respectively, to $P_\ell(z)$ for TE_n and TM_n modes. $P_\ell(z)$ for a given mode (HE_n or HM_n) does not vary much with respect to ψ in the space–guide. Regarding modal field plots, however, there are distinct differences between the HE and the HM modes.

The variation of $e_\perp = \mathbf{e} \bullet \mathbf{u}_\ell$ with respect to z for the HE_n mode is similar in all directions; and, in general, the $e_\perp$ vs. z curves for all HE_n modes resemble those for a TE_n mode in an isotropic interconnect. Thus, all HE_n modes propagating in any direction $\mathbf{u}_\ell$ in a space–guide have similar modal characteristics. However, the $h_\perp$ vs. z plots for the HM_n modes do not display these characteristics. Not only are the $h_\perp$ vs. z plots for an HM_n mode different from that of the TM_n mode, but also the $h_\perp$ vs. z plots are distinctly dissimilar for the various propagation directions. Thus, the dielectric anisotropy and non–homogeneity of the space–guide impart more significant directional dependence to the mode shapes of the HM modes and less to the HE modes.

Clearly, the HE_n mode launched in one direction will not interfere with the HE_n mode launched in some other direction; and the same holds true for any HM_n mode, at least for small values of n. Indeed, several HE and HM modes of low order can be launched in different directions, while taking care that their guide wavenumbers are all different. The space–guide concept is thus well–founded. Obviously, however, hardware requirements will put a limit on the number of channels a TFHBM space–guide can realistically support in actual circuitry.

Acknowledgement
E. Ertekin acknowledges a Graduate Fellowship from the US National Science Foundation.

References

[1] M. S. Sodha and A. K. Ghatak, *Inhomogeneous Optical Waveguides.* New York, NY, USA: Plenum Press, 1977.

[2] I. J. Hodgkinson and Q. H. Wu, *Birefringent Thin Films and Polarizing Elements.* Singapore: World Scientific, 1997.

[3] E. Ertekin and A. Lakhtakia, submitted for publication in *Proc. R. Soc. Lond. A.*

[4] E. Ertekin, *Space–Guides: Efficient Optical Interconnects Made from a Thin–Film Helicoidal Bianisotropic Medium*, M.S. Dissertation. Department of Engineering Science and Mechanics, The Pennsylvania State University (August 2000).